Supporting Online Material for

Chromosome organization by a nucleoid-associated protein in live bacteria

Wenqin Wang, Gene-Wei Li, Chongyi Chen, X. Sunney Xie, and Xiaowei Zhuang

The Supporting Online Material includes

Materials and Methods

1, Strain construction

Homologous recombination. Unless otherwise stated, all strains used in this study were constructed using λ Red recombination developed by Datsenko and Wanner (*44*). The parent strain is BW25993, a derivative of *E. coli* K-12 (*44*). Briefly, linear insertion DNA with flanking homologous sequences was electroporated into BW25993 bearing the plasmid pKD20, which transiently expressed the recombinase. Successful recombination was first selected by an antibiotic resistance marker, followed by PCR screening and sequencing. The selection marker was later removed using the FLP-FRT system (*44*) when appropriate.

Photoactivatable fluorescent protein fusion strains. To create chromosomal fusion of mEos2 and target genes using λ Red recombination, an *mEos2*-CAM cassette was PCR-amplified with primer pairs containing sequences homologous to the desired genes. The *mEos2*-CAM cassette consisted of two pieces: the mEos2-coding sequence, which was codon optimized for expression in *E. coli* and synthesized by Genscript, and the chloramphenicol resistance gene (CAM). In all mEos2-fusion strains reported here, the mEos2 tag is at the C-terminus of the target proteins, and the last codon of the target gene is immediately followed by the start codon of *mEos2*. The PAmCherry1-coding sequence was codon optimized for expression in *E. coli* and synthesized by DNA 2.0, and the fusion strain *hns::PAmCherry1* was constructed in the same way as *hns::mEos2*. Seven fusion strains were constructed as described above and listed in the table below. All of these strains had the same growth rates (cell doubling times) within error as their wildtype parent strain BW25993. Cell doubling times were determined from three independent cultures grown at 37^{o}C in medium supplemented with glucose (see Section 2).

Strain	Genotype	Target labeled	Antibiotic resistance	Doubling time (± SD) (min)
BW25993	Wildtype	None	None	43 ± 3
SX246	*hupA::mEos2*	HU	CAM	43 ± 4
SX249	*hns::mEos2*	H-NS	CAM	46 ± 4
SX250	*fis::mEos2*	Fis	CAM	43 ± 2
SX253	*ihfA::mEos2*	IHF	CAM	46 ± 2
SX254	*stpA::mEos2*	StpA	CAM	45 ± 1
SX289	*rpsV::mEos2*	S22 of Ribosome	CAM	43 ± 3
SX454	*hns::PAmCherry1*	H-NS	CAM	44 ± 4

hns mutants and hns-null strain. Mutations to *hns* were introduced first on a plasmid bearing *hns::mEos2*. The mutated *hns::mEos2*-CAM cassette was then PCR-amplified for homologous recombination. In this way, the following strains were constructed:

Strain	Genotype	Target labeled	Antibiotic resistance

SX280	*hns*^{L30P}::*mEos2*	H-NS^{L30P}	CAM
SX287	*hns*^{P116S}::*mEos2*	H-NS^{P116S}	CAM

To make *hns*-null mutant strain, *hns* gene was replaced by a CAM cassette through the aforementioned homologous recombination.

Strain name	Genotype	Antibiotic resistance
SX270	*hns*-null	CAM

Strains for chromosomal loci labeling. A fluorescent repressor-operator system was used to label specific chromosomal loci in live *E. coli* cells. The system consisted of two parts: *tetO* sites near the locus of interest and the expression of TetR-eYFP. Both parts were inserted into the bacterial chromosome.

To create a low expression system for TetR-eYFP fusion protein, a *tetR::eyfp*-KAN cassette was PCR amplified, consisting of *tetR*::*eyfp* fusion gene and a kanamycin resistance gene (KAN). Using homologous recombination, the cassette was inserted into the chromosome downstream of a lowly expressed gene *malI*. We denote the final construct as *malI-tetR::eyfp*, which is a transcriptional but not translational fusion of *tetR*::*eyfp* to *malI*.

To label specific chromosomal loci, short *tetO* arrays were introduced at the desired loci. We designed a 219 bp DNA consisting of 6 *tetO* sites to allow precise localization of the target gene locus and minimal perturbation to the chromosome. Using homologous recombination, the 6*tetO*-CAM cassette was inserted into the chromosome at the target loci. The antibiotic selection marker (CAM) was removed afterwards using the FLP-FRT system. Specifically, the 6*tetO* array was placed 213 bp, 340 bp and 105 bp upstream of *hdeAB, hchA*, and *lac* operons, respectively. By sequentially inserting the *tetR*::*eyfp* and 6*tetO* arrays into BW25993, we made the following three strains:

Strain	Genotype	Antibiotic resistance
SX372	*malI-tetR::eyfp*, 6*tetO@hdeA*	KAN
SX405	*malI-tetR::eyfp*, 6*tetO@hchA*	KAN
SX319	*malI-tetR::eyfp*, 6*tetO@lacZ*	KAN

Three corresponding *hns*-null strains were additionally generated by introducing *hns* deletion in the above strains:

Strain	Genotype	Antibiotic resistance
SX388	*malI-tetR::eyfp*, 6*tetO@hdeA*, *hns*-null	KAN, CAM
SX413	*malI-tetR::eyfp*, 6*tetO@hchA*, *hns*-null	KAN, CAM
SX365	*malI-tetR::eyfp*, 6*tetO@lacZ*, *hns*-null	KAN, CAM

Two-color strains. For two-color imaging of H-NS and specific gene loci, the strains described in the previous section were further modified with *hns::mEos2* fusion using homologous recombination, generating three new strains as listed below. Their growth rates were also the same as their wildtype parent strain BW25993.

Strain	Genotype	Antibiotic resistance	Doubling time (± SD) (min)
SX292	*malI-tetR::eyfp*, 6*tetO@hdeA*, *hns::mEos2*	KAN, CAM	45 ± 1
SX410	*malI-tetR::eyfp*, 6*tetO@hchA*, *hns::mEos2*	KAN, CAM	45 ± 2
SX259	*malI-tetR::eyfp*, 6*tetO@lacZ*, *hns::mEos2*	KAN, CAM	45 ± 3

2, Cell culture and sample preparation

E. coli cell culture conditions. Prior to imaging, overnight cell culture in Luria broth (LB) was diluted 1:2000 into 2 mL M9 minimal medium supplemented with 0.4% glucose, MEM amino acids and vitamins (Invitrogen). The cells were then incubated in a 37^{o}C shaker for 4-5 hours. The cell doubling time under this condition was measured to be ~45 minutes. When $OD_{600\ nm}$ reached ~0.07 during the early exponential phase, 1 mL of the cell culture was taken out, washed and then resuspended in ~10 μL M9 minimal medium with 0.4% glucose and without any additional supplements for imaging. The imaging sample preparation procedure is described in the next section.

For experiments with glycerol-supplemented medium, M9 minimal medium with 0.4% glycerol without any other supplement was used instead. The cell doubling time under this condition was measured to be ~250 minutes at 37^{o}C. Similarly, 1 mL of the culture was taken out when $OD_{600\ nm}$ reached ~0.07 during the early exponential phase, washed and then resuspended in ~10 μL M9 minimal medium with 0.4% glycerol and without any additional supplements for imaging. The imaging sample preparation procedure is described as follows.

Imaging sample preparation. The FCS2 Closed Chamber System (Bioptechs) was used for live-cell imaging. The cells (cultured, washed and resuspended in the medium as described above) were sandwiched between a coverslip and an agarose gel pad (*45*). The coverslips were cleaned by 30-minute sonication in 1 M KOH, followed by 15-minute sonication in MilliQ water, and finally 10-minute cleaning in a plasma sterilizer. The agarose gel pad was made with 3% agarose (SeaPlaque GTG Agarose Cat # 50111, Lonza) dissolved in M9 minimal medium with 0.4% glucose (or 0.4% glycerol). The chamber containing cells was assembled 0.5 – 2 hours before imaging and maintained at room temperature. The cell doubling times under these imaging conditions were substantially longer than the double times observed under the culture conditions described in the previous section.

3, Imaging setup and procedure

Objectives and focus stabilization. Single-molecule and super-resolution imaging were performed on an Olympus IX-71 inverted microscope with a 100× UPlanSApo, NA 1.4 Olympus oil immersion objective, or a 100× UPlanApo, NA 1.35, Olympus oil immersion phase objective. The latter objective was used in the cases where phase-contrast images were used to map out the cell contours. When needed, the focus of the objective was maintained by an active stabilization system consisting of an infrared 830 nm laser (LPS-830-FC, Thorlabs) and a quadrant photodiode. The reflected 830 nm signal from the sample was detected by the quadrant photodiode and used as feedback to control the objective focus position. The focus stabilization system is similar to previous implementations in the lab (*32,46*).

Excitation path. Three lasers of different wavelengths were used: a 405 nm laser (CUBE 405-50C, Coherent) to photoactivate mEos2 (or PAmCherry1), a 561 nm laser (Sapphire 561-200 CW, Coherent) for imaging photoactivated mEos2 (or PAmCherry1), and a 514 nm laser (Sapphire 514-50 CW, Coherent, or Innova 300, Coherent, with an exciter D510/20X by Chroma) for imaging eYFP. The "on" and "off" states of these laser lines were controlled either by electronically controlling the laser power supply or by mechanical shutters (Uniblitz LS6T2, Vincent Associates). The laser intensities were adjusted electronically either by the laser power supply (for the 405 nm laser) or by an acousto-optic tunable filter (Chrystal Technology, for all the other lasers). The power densities at the sample were 0.1 - 100 W/cm^2 at 405 nm, 0.2 kW/cm^2 at 514 nm, or 2 kW/cm^2 at 561 nm. The 405 nm activation laser intensity was gradually increased during super-resolution image acquisition in order to compensate for photobleaching and to maintain a roughly constant density of activated molecules. All laser beams were combined by dichroic mirrors and coupled into a custom optical fiber (Oz Optics). The output light from the optical fiber was collimated and subsequently focused at the back focal plane of the objective.

Emission path. Fluorescence emission was collected through the afore-described objectives, separated from the excitation lasers using a dichroic or polychroic mirror, filtered by emission filters before being relayed by a two-channel system (DV-CC Dual-view, Photometrics), and then imaged onto an EMCCD camera. The two-channel system was set to single-channel configuration for single-color imaging. In the case of 3D imaging, a 1 m focal length cylindrical lens (LJ1516L1-A, Thorlabs) was inserted in the imaging path.

In the case of single-color mEos2 (or PAmCherry1) imaging, a dichroic mirror Di01-R561 (Semrock), a band pass emitter FF01-617/73 (Semrock), and an Ixon DV897DCS-BV camera (Andor) were used. In the case of single-color eYFP imaging, a 514 nm dichroic, a HQ545/30m emitter, and a Cascade 512B camera (Photometrics) were used. In the case of two-color imaging of eYFP and mEos2, a polychroic filter z405/514/561rpc (Chroma) was used to separate the emission from excitation lasers, and an additional 561 nm notch filter (NF03-561E-25, Semrock) was used to block the residual 561 nm light. The emissions of eYFP and mEos2 were then split by a dichroic (FF570-Di01, Semrock), and separately filtered by a band pass filter: FF01-542/27-25 (Semrock) for eYFP or FF01-617/73-25 (Semrock) for mEos2, and finally detected by the

Ixon DV897DCS-BV camera. Fiducial markers that appear in both color channels (100 nm-diameter fluorescent beads, T-7279, Invitrogen) were used for two-channel mapping.

The super-resolution images of mEos2-labeled NAPs were acquired at 60 Hz for up to 7,200 frames. The super-resolution images of PAmCherry1-labeled H-NS were acquired at 30 Hz for 3,600 frames. Of these movies, only the first 0.5 or 1 min was used for H-NS cluster size analysis. The eYFP-labeled gene loci were acquired at 10 Hz for 1 frame for the single-color images, and at 10 Hz for 50-100 frames for the two-color images.

4, Image data analysis

Super-resolution image construction and image resolution. Image analysis was performed in a similar manner as described previously (*32,46,47*). Briefly, fluorescence peaks of individual molecules were identified and fit to a 2D elliptical Gaussian to determine each peak's centroid position (x, y) and ellipticity. For 3D images obtained with the cylindrical lens, the z-coordinate of each localization was determined by comparing the obtained ellipticity with a predetermined calibration curve of ellipticity versus z as described previously (*32,46*). The average photon number detected from the activated mEos2 molecules before photobleaching was ~1300 and only localization events with more than 300 photons were accepted. The photobleaching rate of mEos2 under our imaging condition was comparable to the camera frame rate (60 Hz) and therefore slightly more than half (52%) of the activated molecules were fluorescent for one frame only. For molecules that lasted for more than one frames, their average localizations from multiple frames were used in the super-resolution images. A smaller number of photons (~1000) were detected from the activated PAmCherry1 molecules before photobleaching.

Sample drift was calculated by correlating the super-resolution images constructed in different time segments to that at the beginning of the movie, and then subtracted as described previously (*32,46*). Since the wide-field image is comprised of many cells, this image correlation approach only subtracts the overall sample drift, but not the movements of individual molecular structures inside each cell, which is not correlated across the whole field of view.

To determine the localization precision of mEos2, fluorescent beads were imaged over the same duration using the same configuration as mEos2 imaging. The emission from each bead was partitioned into equal time segments with ~1300 photons detected per segment on average to match the average photon numbers detected from individual mEos2 molecules. The bead position was determined within each time segment and a localization distribution was determined for each bead. The average distribution width (full-width-at-half-maximum) was used to define the localization uncertainty. Using this method, we determined the localization precision to be ~35 nm in the xy plane and ~75 nm along the z direction. Since our ability to localize the molecules precisely could also be affected by their movement, we assessed this effect by examining those mEos2-labeled H-NS molecules that were fluorescent for more than one consecutive frames and determining their positions in each frame. The frame-to-frame

localization uncertainty measured this way was ~35-40 nm (in *xy*), comparable to the localization precision determined above using fixed beads, suggesting that our localization precision in each imaging frame was not substantially affected by molecular movement.

For two color imaging, a 3rd order polynomial transformation was used to map the two color channels based on images of fiducial markers (fluorescent beads) that appeared in both color channels. The alignment residuals were < 8 nm.

H-NS cluster size characterization. H-NS clusters in the super-resolution images were automatically segmented by calculating the local density of localizations and indentifying all peaks on this density map that were above a threshold value. We chose the threshold value based on the following analysis. First, we found the least stringent threshold value to identify all the clusters without falsely connecting them. We then constructed the histogram of the full-width-at-half-maximum (FWHM) sizes from all identified clusters. The histogram clearly showed a bimodal distribution, with two populations of clusters separated by a pronounced gap. The major population included clusters with FWHM sizes larger than ~100 nm, which accounted for the vast majority of clusters (80%) and nearly all (96%) the localizations in identified clusters. The much minor population of smaller clusters contributed a mere 4% of the clustered localizations. To focus on the major population which included nearly all clustered molecules, we re-adjusted the threshold value to minimize the contribution from the minor population without significant perturbation to the major population. An example of the cluster segmentation result is shown in Fig. 2E inset.

To characterize the cluster size, a 2D distribution was constructed for localizations in each cluster, which was then fit to an elliptical Gaussian to determine the distribution widths along both the long and short axes. The cluster size is defined as the geometric mean of the width values along the two axes. Two criteria were used to determine the width. One is the commonly used full width at half maximum (FWHM, Fig. 2E bottom axis). The other is the full width at 3% maximum (Fig. 2E top axis), considering that the average localization density outside the clusters was only ~1% of the peak densities inside the clusters.

Estimating the fraction of H-NS molecules in the clusters. To determine this fraction, we defined the boundary of a cluster as the contour where the localization density is 3% of the peak localization density of the cluster. We then constructed a sum of the activated mEos2 images associated with molecules within the cluster boundaries and determined the total fluorescence signal from this sum image, denoted as $I_{cluster}$. Next, we measured the total fluorescence signal of all activated mEos2 molecules within the cells, denoted as I_{total}. I_{total} should include signals from molecules localized with the clusters, molecules localized outside the clusters, as well as molecules that were too dim or diffused too fast to be imaged and localized at the single-molecule level. The fraction of H-NS molecules in the clusters was then calculated from $I_{cluster}$ / I_{total}. According to this analysis, 60 ± 25% of H-NS molecules resided in the clusters. The number of H-NS molecules in the clusters per cell can be estimated by multiplying this fraction

and the total number of H-NS molecules per cell obtained from quantitative Western blot experiments (see Table S1). We note that this analysis using the 3% boundary slightly underestimate the actual fraction of molecules in the clusters, since the average localization density outside the clusters was only ~1% of the peak densities of the clusters. However, the underestimate is very moderate -- changing the boundary definition to the 2% contour line only changed the fraction by 1%.

Determining H-NS cluster and gene locus positions relative to the cell axes. The position of each H-NS cluster was determined by calculating the average of localizations in each cluster. The eYFP-labeled gene locus positions were obtained by fitting individual eYFP fluorescence images to 2D Gaussians to determine the centroid positions. In order to identify the outline of each cell, phase-contrast images of cells were filtered and thresholded to create binary images, which were then automatically segmented to contiguous areas (*24*). These areas were screened based on their sizes and aspect ratios to exclude falsely identified cell debris and overlapping cells. The segmented areas were then fit with a 2D elliptical function to determine the long and short axes of the cells. The relative position of the H-NS clusters and gene loci to the cell axes were then determined.

Analysis of co-localization between the H-NS clusters and the gene loci. H-NS clusters were automatically segmented as described above. For each gene locus detected, its nearest H-NS cluster was identified. The cluster-locus pairs were then aligned according to the center position of each cluster and the line connecting the cluster center and the locus position. The summed localization distributions of all the aligned clusters are plotted as the magenta curves and the distributions of the distance between the cluster center and the locus position are plotted as the green curves in Fig. 3C. The curves in Fig. 3C allows the different levels of colocalization with H-NS clusters to be compared between *hdeA*, *hchA*, and *lacZ* without the need to assign any threshold value to identify cluster boundaries. To give a single percentage number of the colocalization fraction in each case, we again defined the boundary of a cluster as the contour line where the localization density is 3% of the peak localization density of the cluster. Based on the 3% line (grey lines) on the average H-NS profile (magenta curves) in Fig. 3C, we determined that 67% of *hdeA*, 65% of *hchA*, and 36% of *lacZ* loci resided in the H-NS clusters. We note that the colocalization fraction of *lacZ* is not much higher than the expected background value (20-30%) derived from a random distribution of the gene locus in the nucleoid.

Because of the heterogeneity in the H-NS cluster size, the above estimate using the average profiles of H-NS clusters may overestimate the colocalization fractions. We thus also determined the colocalization fractions using an alternative single-locus-based analysis. In this approach, we determined colocalization between each individual gene locus and its nearest H-NS cluster, again using the 3% peak density to define the boundary of each cluster. Using this single-locus-based analysis, we determined that 43% of *hdeA*, 41% of *hchA*, and 20% of *lacZ* loci resided in the H-NS clusters. While the colocalization fractions obtained from this analysis are moderately

smaller than the ensemble analysis described above, the difference between *hdeA*/*hchA* and *lacZ* is similar to that from the ensemble analysis.

Again, these analyses using the 3% peak localization density to define the cluster boundary slightly underestimate the colocalization fraction since the average localization density outside the clusters was only ~1% of the peak densities of the clusters. However, the underestimate is again moderate -- changing the boundary definition to the 2% contour line only changed the colocalization fractions by a few percent.

5, Quantitative Western blot

Concentration standard. HU and H-NS protein solutions used as concentration standards for quantification were prepared as follows. *hupA* and *hns* genes were inserted into a pET30a plasmid with a C-terminal His-tag, and transformed into BL21(DE3)pLysS competent cells (Invitrogen). After IPTG induction, His-tagged proteins were purified by His-Spin Protein Miniprep Kit (Zymo Research). The protein purity was validated using sodium dodecyl sulfate polyacrylamide gel electrophoresis (SDS-PAGE) and Coomassie blue staining. The final concentration was determined by Quick Start Bradford Protein Assay (Bio-Rad Laboratories).

Western blot. To determine the amount of H-NS and HU proteins per cell, the cell culture was harvested under the same condition as in the imaging experiments, with the cell number estimated by LB agar plating. The concentration standard and the cell culture resuspension were heat-denatured and separated by SDS-PAGE using 4-15% Tris-HCl Ready Gel PAGE gel (Bio-Rad Laboratories), and transferred to Hybond-P PVDF membrane (GE Healthcare). The polyclonal anti-HU antibody (provided by Professor Jon Kaguni) (*48*), monoclonal anti-H-NS antibody (provided by Professor Jay Hinton) (*49*), and polyclonal anti-DsRed2 antibody (Clontech) were used to detect HU, H-NS, and mEos2, respectively. These primary antibodies were then recognized by Cy5-labeled goat-anti-rabbit or goat-anti-mouse secondary antibodies (GE Healthcare). Typhoon TRIO Scanner (Amersham Biosciences) and the ImageQuant TL software were used to quantify Western blot results.

6, mRNA expression level measurement by reverse transcription (RT)-qPCR

RNA extraction. The total RNA was extracted under the same culture condition as in the imaging experiments. One-tenth of the sample volume of cold 90:10 ethanol:phenol mixture was directly added to the cell culture. The harvested cells were washed twice with cold phosphate buffered saline (PBS) followed by 10-min 25 μg/mL lysozyme digestion in Puregene Cell Lysis Solution (Gentra Systems) at room temperature. From the cell lysate, RNA was extracted by phenol chloroform iso-amyl alcohol (PCIAA) pH 4.5 (Ambion) and further purified by isopropanol precipitation and 70% ethanol wash. Finally, the air-dried RNA pellet was resuspended to a concentration of 100 μg/mL, and RNase-free DNase I (New England BioLabs) was added to a final concentration of 40 U/mL for 30-min incubation at 37^{o}C. Next, EDTA was

added to a final concentration of 5 mM for 10-min incubation at 75^{o}C. The RNA solution was further purified using an RNA purification kit (RNA Clean & Concentrator-25, Zymo Research), and the purified RNA concentration was determined by measuring the absorption with a spectrophotometer (NanoDrop 2000, Thermo Scientific).

cDNA preparation. The total RNA was converted to cDNA using M-MuLV reverse transcriptase with random hexamer primers. A master mix was made by mixing 1 μg RNA solution, 0.1 nmol random hexamers (Applied Biosystems), 10 nmol dNTP, together with nuclease-free water to a final volume of 16 μL, and then incubated at 70^{o}C for 5 min. Next, 1 μL 20 U/μL RNase inhibitor (Applied Biosystems), 1 μL 200 U/μL M-MuLV reverse transcriptase (New England BioLabs), and 2 μL 10X M-MuLV reverse transcription buffer were added to the mixture to make a final 20 μL reaction mix. The reaction mix was incubated at room temperature for 10 min, then at 42^{o}C for 60 min, and finally at 90^{o}C for 10 min. The final cDNA product was stored at -80^{o}C.

qPCR quantification. qPCR was carried out using DyNAmo™ HS SYBR Green qPCR kit (Finnzymes) and ABI Fast 7500 Real-Time qPCR machine (Applied Biosystems) following manufacturer instructions. A non-template control was included for each primer pair. The product integrity was checked using the dissociation curve. Cycle Threshold (C_t) was read out, and the starting template amount was quantified based on the value of C_t assuming exponential growth at early stages of amplification. All samples were normalized by internal control signals. The following primers were used:

hdeA
hdeA36f 5'-GCTTCTTCTGCCAGTTGTGAGCAA-3'
hdeA132r 5'-AGCCAGGAAATCTTCACAGGTCCA-3'
hchA
hchA320f 5'-GGGCTATGCCGCACAAAGATGAAA-3'
hchA462r 5'-ACCACCAGGAACAAAGATTGCTGC-3'
lacZ
lacZ1657f 5'-TACTGGCAGGCGTTTCGTCAGTAT-3'
lacZ1832r 5'-TCGGCAAAGACCAGACCGTTCATA-3'
***ssrA* (Internal Normalization Control)**
ssrA191f 5'-AAAGAGATCGCGTGGAAGCC-3'
ssrA341r 5'-ACCCGCGTCCGAAATTCCTA-3'

7, Chromosome Conformation Capture (3C) assay

DNA crosslinking and cell lysis. The cell culture was prepared under the same condition as in the imaging experiments. 100 mL of the cell culture was washed by 1 mL PBS and resuspended in 315 μL PBS. 190 μL 3.2% PBS-diluted formaldehyde (32% formaldehyde, #15714, Electron Microscopy Sciences) was added to the resuspension at room temperature for 30 min, and then

placed on ice for another 30 min for crosslinking reaction. For non-crosslink control, the formaldehyde was replaced by 190 μL PBS. At the end of the incubation, 25 μL 2.5 M glycine solution was added to all samples, thereby quenching the reactions for crosslinked samples.

To subsequently lyse the cells, each sample was spun down at 13,000 rpm, 4^{o}C for 3.5 min and resuspended in 466 μL TE buffer (pH 8.0). Next, 1.4 μL 35 KU/ μL Ready-Lyse lysozyme (Epicentre Biotechnologies) was added to the resuspension and incubated at room temperature for 20 min. Next, 25 μL 10% SDS solution was added for 30-min incubation at room temperature. The cell lysate was stored at -80^{o}C before being digested.

Digestion and ligation. The cell lysate (50 μL) was added to the 470 μL digestion mixture, which was made from 53 μL 10X EcoRI digestion buffer, 53 μL 10% Triton X-100, and 364 μL MilliQ water. After incubation at room temperature for 20 min, 10 μL 100 U/ μL digestion enzyme EcoRI (New England BioLabs) was added for 5-hour digestion at 37^{o}C.

After the digestion, ligation was performed by adding the 530 μL reaction mix to 7.7 mL ligation mixture which contained 6 mL MilliQ water, 745 μL 10% Triton X-100, 20 μL 10 mg/mL bovine serum albumin, 53 μL 10 mM ATP, 766 μL 10X T4 DNA ligation buffer, and 10 μL 2000 U/ μL T4 DNA ligase (New England BioLabs). The ligation reaction was incubated at 16^{o}C for at least 6 hours, followed by 30-min incubation at room temperature. Proteinase K was added to the sample and incubated overnight to stop the ligation reaction.

DNA purification. To remove RNA from the samples, 10 μL 100 mg/mL RNase A (Qiagen) was added for 2-hour incubation at 37^{o}C for each sample. DNA was extracted by equal volume of PCIAA pH 7.9 (Ambion) twice and then pure chloroform once. To precipitate DNA, we used glycogen (final concentration 50 μg/mL, Affymetrix), 32 μL 3 M sodium acetate, and 400 μL isopropanol, per 400 μL DNA solution. Finally, the air-dried DNA pellet was hydrated with MilliQ water for qPCR quantification.

qPCR quantification. To quantify the amount of ligated DNA, qPCR with primers designed for specific chromosomal loci was performed, using the same protocol as in mRNA RT-qPCR assay in Section 6. The following primers were used:

A: *gadA* 5’-TGGGTTATCTGGCGTGACGAAGAA-3’
B: *gltF* 5’-ATGCCGCATTTGCCAGAAAACAAC-3’
C: *ygeH* 5’-GTGCAGTTAACCACTATAACCAGCACC-3’
D: *fliA* 5’-CGCAATTTGTCAGCAACGTGCTTC-3’
E: *ydeO* 5’-AGTACTGAGCGGAGTTTCTTACAGCT-3’
F: *yccE* 5’-GCTCCTGTAGATGGCGATGGATATTGTC-3’
G: *appY* 5’-ACGATCTTTCTTCCTCCGTTGCGA-3’
H: *yahA* 5’-GCAGCTTGAGTAGCAGTCGTTCTTTC-3’
I: *arpA* 5’-TTGTGCAGCAATGTGTCGGCATAC-3’
a: 3196k 5’-GGGTGTTTGGATCGAGCAATTCATCC-3’

b: 1684k 5’-GGCTTTTGTTCACGTCGTCGTTAGG-3’
c: *lacZ* 5’-AACAGCAACTGATGGAAACCAGCC-3’
d: 3800 5’-GAAAGATCACAACGAGCAGGTCAGC-3’
***hchA* (Internal normalization control)**
hchA320f 5’-GGGCTATGCCGCACAAAGATGAAA-3’
hchA462r 5’-ACCACCAGGAACAAAGATTGCTGC-3’

All the qPCR results were validated by regular PCR and DNA electrophoresis.

Supporting Table and Figures

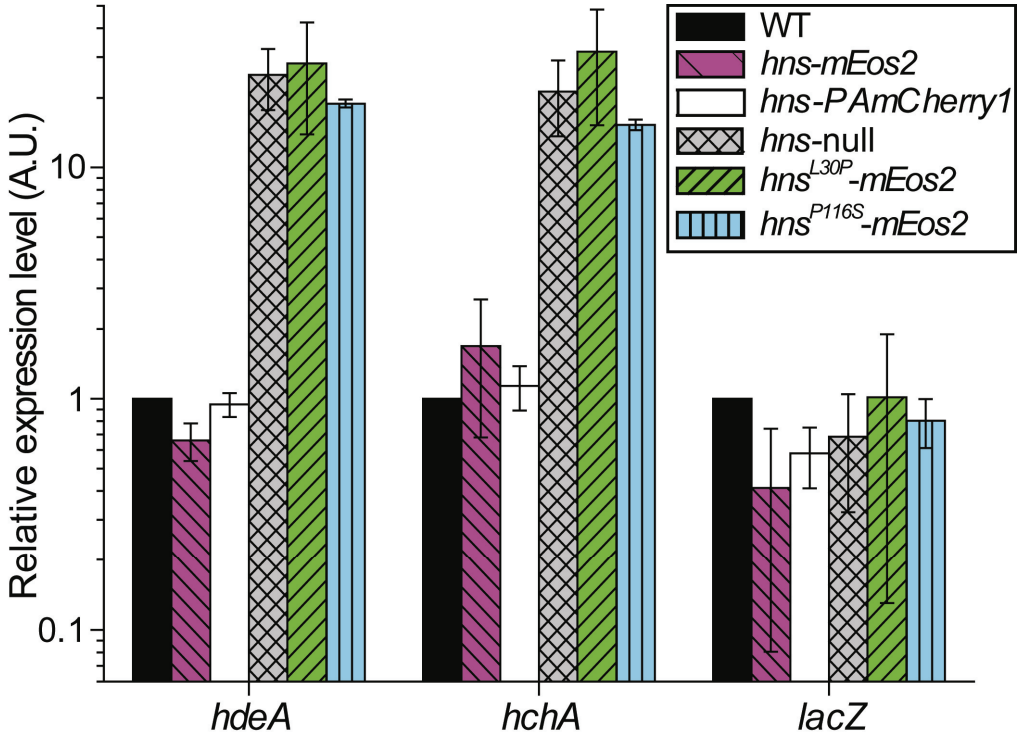

Fig. S1. The relative expression levels of the messenger RNAs of *hdeA*, *hchA* and *lacZ* in the wildtype strain, *hns::mEos2* fusion strain, *hns::PAmCherry1* fusion strain, *hns*-null mutant strain, hns^{L30P}*::mEos2* mutant strain, and hns^{P116S}*::mEos2* mutant strain. The mRNA levels were measured by RT-qPCR. The expression levels for each gene in various strains were normalized by that in wildtype cells. The error bars are SD ($N = 3$).

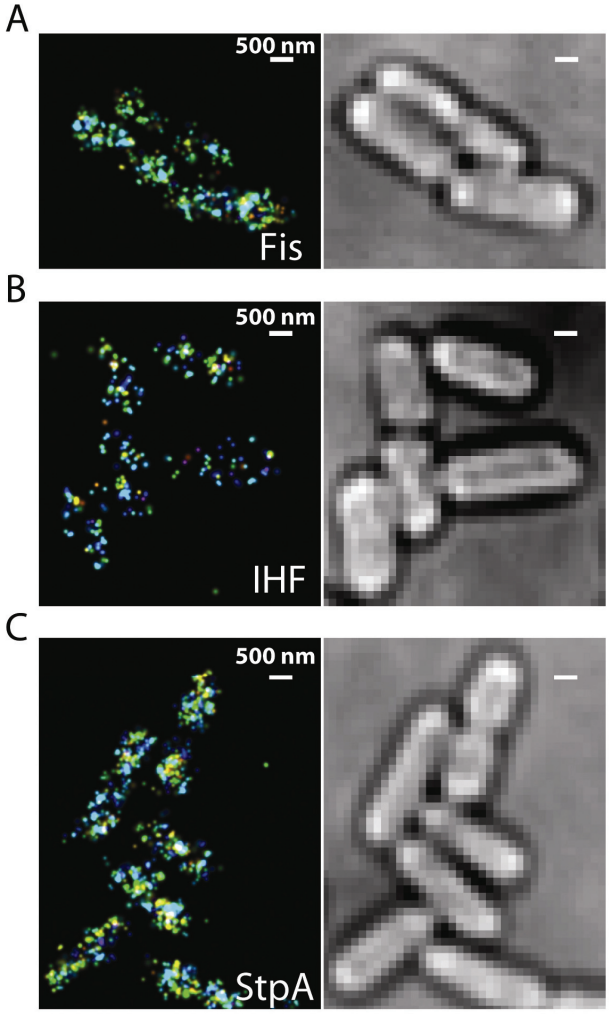

Fig. S2. Distributions of Fis, IHF, and StpA in live *E. coli* cells. Fis (A), IHF (B), and StpA (C) proteins were labeled with mEos2. The left panels show the 3D super-resolution images of the proteins and the right panels show the bright-field images of the corresponding cells. The *z*-coordinates of the molecules are color-coded according to the color bar in Fig. 1.

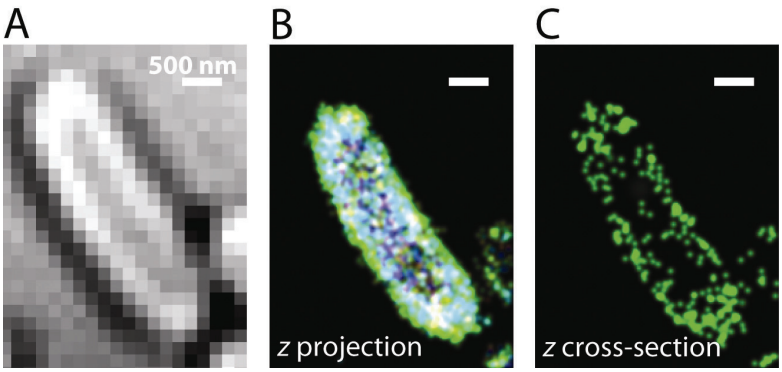

Fig. S3. Distribution of ribosomes in live *E. coli* cells. We labeled the ribosome by fusing a ribosomal subunit protein S22 with mEos2. (A) Bright-field image of the cell. (B) 3D super-resolution image of the ribosomal S22 proteins with *z*-coordinates color-coded according to the color bar in Fig. 1. (C) A 50 nm-thick *z* cross-section of the 3D image showing the enrichment of the ribosomes in the cell periphery and a central void rarely populated by the ribosomes.

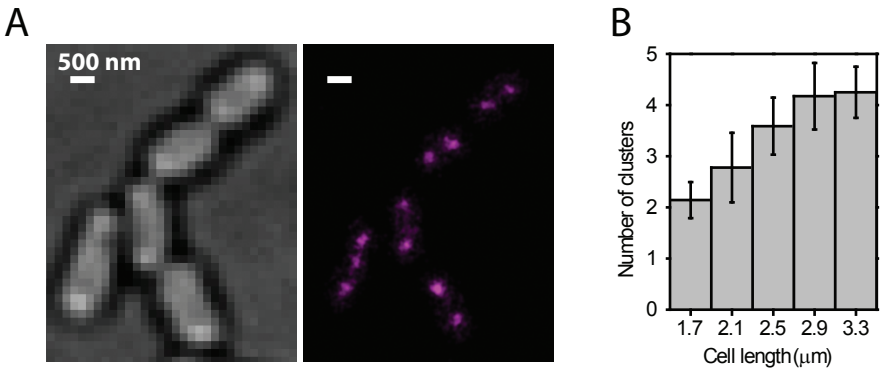

Fig. S4. Super-resolution imaging of H-NS labeled with PAmCherry1 in live cells. (A) PAmCherry1-labeled H-NS forms compact clusters in the nucleoid similar to the mEos2-labeled H-NS. Left, bright-field image of cells. Right, super-resolution image of H-NS tagged by PAmCherry1. (B) The average number of clusters per cell versus the cell length for cells grown in medium supplemented with glucose. Error bars: SD (N = 77, 36, 35, 23, and 4 cells from left to right).

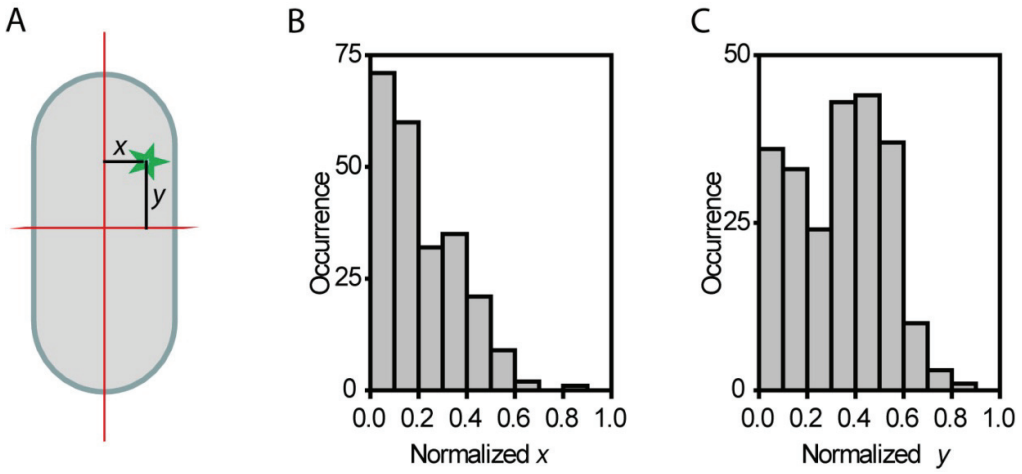

Fig. S5. Spatial distribution of H-NS clusters in cells containing three clusters. (A) Scheme for measuring H-NS cluster localization. The centroid coordinate (x, y) of each H-NS cluster (green star) was determined relative to the cell axes (red lines). (B) The distribution of x normalized to the half cell width. (C) The distribution of y normalized to the half cell length.

Target protein	Antibody used	Protein copy number per cell (± SD)
Wildtype HU	Anti-HU	9,267 ± 2,802
HU-mEos2	Anti-HU	23,400 ± 3,396
Wildtype H-NS	Anti-H-NS	13,533 ± 4,801
H-NS-mEos2	Anti-H-NS	27,067 ± 3,807
H-NS-PAmCherry1	Anti-H-NS	21,333 ± 5,805
H-NS-mEos2	Anti-mEos2	100%
$H\text{-}NS^{P116S}$-mEos2	Anti-mEos2	118% ± 14%
$H\text{-}NS^{L30P}$-mEos2	Anti-mEos2	55% ± 20%

Table S1. Protein copy number estimation by quantitative Western blot. HU proteins were probed by anti-HU antibody in both wildtype (Row #1) and *hupA::mEos2* fusion (Row #2) strains. H-NS proteins were probed by anti-H-NS antibody in wildtype (Row #3), *hns::mEos2* fusion (Row #4), and *hns::PAmCherry1* fusion (Row #5) strains. To compare the expression levels of $H\text{-}NS^{P116S}$ and $H\text{-}NS^{L30P}$ mutants to the wildtype H-NS, because H-NS antibody may not bind the wildtype protein and mutants with the same affinity, the mEos2 fusion proteins were probed by anti-mEos2 antibody in *hns::mEos2*, hns^{P116S}*::mEos2* and hns^{L30P}*::mEos2* strains. The amounts of $H\text{-}NS^{P116S}$-mEos2 and $H\text{-}NS^{L30P}$-mEos2 proteins per cell in the mutant strains (Rows #7 and #8) were determined relative to the amount of H-NS-mEos2 protein in the *hns::mEos2* strain (which is set to 100% in Row #6). The errors are standard deviations (SD) determined from three independent sets of experiments.

Supporting Movie Caption

Movie S1. Time lapsed movie of H-NS clusters in live *E. coli* cells. Each snapshot in the movie is acquired with 60-sec imaging time. The movie is created with a running window scheme such that the consecutive snapshots are 1 sec apart from each other. Scale bar: 500 nm. The *z*-coordinate of each localization is color-coded according to the color bar in Fig. 1.

References

44. K. A. Datsenko, B. L. Wanner, *Proc Natl Acad Sci U S A* **97**, 6640 (2000).
45. J. E. J. Xiao, G.-W. Li, J. YU, X. S. Xie, in *Single Molecule Techniques: A Laboratory Manual,* P. Selvin, T. Ha, Eds. (Cold Spring Harbor Laboratory Press, 2007), pp. 149-170.
46. B. Huang, S. A. Jones, B. Brandenburg, X. Zhuang, *Nat Methods* **5**, 1047 (2008).
47. M. Bates, B. Huang, G. T. Dempsey, X. Zhuang, *Science* **317**, 1749 (2007).
48. S. Chodavarapu, M. M. Felczak, J. R. Yaniv, J. M. Kaguni, *Mol Microbiol* **67**, 781 (2008).
49 J. M. Sonnenfield, C. M. Burns, C. F. Higgins, J. C. Hinton, *Biochimie* **83**, 243 (2001).